Octave-spanning mid-infrared supercontinuum generation in silicon nanowaveguides

Ryan K. W. Lau,[1,*] Michael R. E. Lamont,[1,2,3] Austin G. Griffith,[3] Yoshitomo Okawachi,[1] Michal Lipson,[2,3] and Alexander L. Gaeta[1,2]

[1]*School of Applied and Engineering Physics, Cornell University, Ithaca, New York 14853, USA*

[2]*Kavli Institute at Cornell for Nanoscale Science, Ithaca, New York 14853, USA*

[3]*School of Electrical and Computer Engineering, Cornell University, Ithaca, New York 14853, USA*

**Corresponding author: rkl48@cornell.edu*

Received May 21, 2014; accepted June 2, 2014;
posted June 20, 2014 (Doc. ID 212442); published July 28, 2014

We report, to the best of our knowledge, the first demonstration of octave-spanning supercontinuum generation (SCG) on a silicon chip, spanning from the telecommunications c-band near 1.5 μm to the mid-infrared region beyond 3.6 μm. The SCG presented here is characterized by soliton fission and dispersive radiation across two zero group-velocity dispersion wavelengths. In addition, we numerically investigate the role of multiphoton absorption and free carriers, confirming that these nonlinear loss mechanisms are not detrimental to SCG in this regime.

OCIS codes: (130.3060) Infrared; (320.6629) Supercontinuum generation; (190.4390) Nonlinear optics, integrated optics.

http://dx.doi.org/10.1364/OL.39.004518

Supercontinuum generation (SCG) is characterized by spectral broadening of ultrashort pulses, with applications in frequency metrology, optical coherence tomography, microscopy, and optical communications. Photonic waveguides can greatly facilitate broadband SCG due to a combination of enhanced nonlinearity and dispersion tailoring. While significant work on broadband SCG has been performed in microstructured optical fibers [1–5], the drive for an integrated, chip-based solution has led to the emergence of several attractive platforms, including chalcogenide glass [6,7], high-index glass [8], silicon nitride [9], and silicon [10–12]. Silicon waveguides are particularly attractive, benefiting from a large effective nonlinearity, compact device footprint, and complementary metal-oxide-semiconductor (CMOS) compatibility. Furthermore, there has been recent interest in extending the operation of these devices to the mid-infrared (MIR) wavelength region, as it has been shown that the nonlinear loss mechanism of two-photon absorption (TPA) vanishes beyond 2.2 μm [13,14]. For example, wavelength conversion based on four-wave mixing has been demonstrated using a 2 μm pump [15,16], enabling MIR wavelengths to be addressed by traditional telecom sources and detectors. In addition, large parametric gain [17,18] has been observed.

It is well known that pumping in the anomalous wavelength region near the zero group-velocity dispersion (ZGVD) wavelength may result in broadband SCG predominantly governed by soliton fission and dispersive wave generation [5]. Furthermore, it has been shown theoretically and experimentally that under suitable conditions, a second ZGVD wavelength on the opposite side of the pump will result in even broader SCG due to the generation of redshifted dispersive waves [3,4]. While silicon-based SCG in the MIR wavelength range has been previously demonstrated [11,12], the generated spectrum was limited to 990 nm, as the spectral broadening was mainly due to modulation instability with a single dispersive wave at lower wavelengths.

In this Letter, we present a fundamentally different SCG, characterized by soliton fission and dispersive radiation across both ZGVD wavelengths, which enables us to achieve MIR spectra spanning 1.3 octaves, from 1.51 to 3.67 μm, in a silicon wire waveguide. This demonstration represents, to the best of our knowledge, the first octave-spanning SCG from a silicon chip.

The silicon-on-insulator (SOI) waveguide used in our experiments has a cross section of 320 nm by 1210 nm, and a length of 2 cm, and is engineered to exhibit a ZGVD wavelength on each side of the 2.5 μm pump. Figure 1 shows the group-velocity dispersion (GVD) of the waveguide for the fundamental transverse electric (TE) mode, modeled using a custom finite-difference mode solver. The GVD is anomalous within the tuning range of the pump and falls to zero near 2.1 and 3.0 μm. The waveguide cross section and mode profile at $\lambda = 2.5$ μm are shown in the inset.

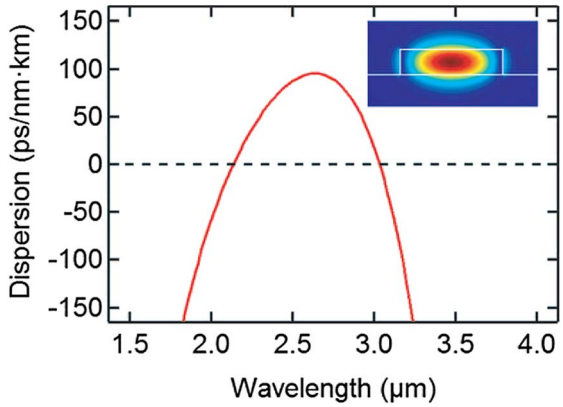

Fig. 1. Simulated group-velocity dispersion (GVD) curve for fundamental TE mode of an SOI waveguide with a cross section of 320 nm by 1210 nm, which results in anomalous GVD near the pump wavelength of 2.5 μm and zero-GVD wavelengths near 2.1 and 3.0 μm. The waveguide cross section and the mode profile are shown in the inset.

The waveguide is fabricated as described in Ref. [16]. It is pumped near 2.5 μm with 300 fs pulses from an optical parametric oscillator (OPO) at a repetition rate $R_p = 80$ MHz. The pulses have an average power of 3 mW and are coupled into and out of the waveguide using aspheric chalcogenide lenses. The peak power of the OPO idler output is 125 W, and with an input coupling loss of 9 dB, we estimate an on-chip peak power of approximately 15 W. The output spectra are measured using a Fourier transform infrared spectrometer (FTIR) with a liquid nitrogen-cooled InSb detector.

Figure 2 shows the output spectra as the pump wavelength is tuned away from the normal-GVD regime near 2.1 μm. We observe spectral broadening of more than 1000 nm near the pump and the generation of dispersive waves near 1.5 and 3.6 μm. As the pump wavelength is further tuned toward the peak anomalous GVD regime near 2.5 μm, we observe the corresponding shift of both dispersive waves. The telecom dispersive wave blueshifts since the pump is moving farther away from the ZGVD wavelength at 2.1 μm, and the MIR dispersive wave redshifts since the pump is moving closer to the ZGVD wavelength at 3.0 μm, as expected due to phase matching conditions [5].

Although we are operating in the wavelength region beyond 2.2 μm, where TPA can be neglected [13], three-photon absorption (3PA) may have a non-negligible effect. We model the pulse evolution in the silicon waveguide using the following nonlinear Schrodinger equation, which is modified to include 3PA and the free-carrier effects [19–21]:

$$\frac{\partial A}{\partial z} = -\frac{\alpha}{2}A + \sum_{m\geq 2} i^{m+1}\frac{\beta_m}{m!}\frac{\partial^m A}{\partial \tau^m} + \left(1 + \frac{i}{\omega_0}\frac{\partial}{\partial \tau}\right)\left(i\gamma|A|^2 A - \frac{\gamma_{3\,\mathrm{PA}}}{3A_{\mathrm{eff}}^2}|A|^4 A\right) - \frac{\sigma}{2}(1+i\mu)N_c A, \tag{1}$$

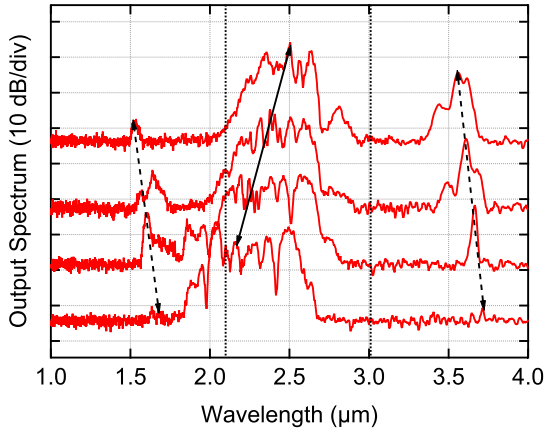

Fig. 2. Experimentally measured output spectra as the pump is tuned from 2.165 to 2.501 μm, as indicated by the solid line. From bottom to top, the spectra correspond to pump wavelengths of 2.165, 2.251, 2.373, and 2.501 μm, respectively. Dashed lines show the resulting shift of dispersive waves generated near 1.5 and 3.6 μm. Zero-GVD wavelengths at 2.1 and 3.0 μm are indicated by dotted lines.

where $A(z,t)$ is the envelope of the electric field, α is the linear loss, β_m are the dispersion coefficients at the central frequency ω_0 of the pulse, $\tau = t - \beta_1 z$ is the retarded time, $\gamma = \omega n_2/cA_{\mathrm{eff}}$ is the nonlinearity of the waveguide, n_2 is the nonlinear index coefficient, A_{eff} is the effective area of the waveguide mode, $\gamma_{3\mathrm{PA}}$ is the 3PA coefficient, and σ and μ are the free-carrier absorption (FCA) cross section and free-carrier dispersion (FCD) parameters, respectively. The free-carrier density N_c is modeled by the rate equation

$$\frac{\partial N_c}{\partial t} = \frac{\gamma_{3\mathrm{PA}}}{3h\nu_0}\frac{|A|^6}{A_{\mathrm{eff}}^3} - \frac{N_c}{\tau_{\mathrm{eff}}}, \tag{2}$$

where τ_{eff} is the effective carrier lifetime. We numerically solve Eqs. (1) and (2) using the split-step Fourier method [19], with values $n_2 = 9\times10^{-14}$ cm^2/W, $\gamma_{3\mathrm{PA}} = 0.025$ cm^3/GW^2, $\sigma = 3.7\times10^{-21}$ m^2, and $\mu = 4.7$, as taken from the literature [22–24]. We use a value of 10 ns for the free-carrier lifetime, taken as an upper estimate from the measurements of smaller but similar devices [25].

The spectral and temporal evolution of an input hyperbolic secant pulse are simulated and presented in Figs. 3(a) and 3(b). We observe an initial stage of spectral broadening and temporal compression followed by soliton fission halfway along the 2 cm waveguide and the subsequent formation of short-wavelength and long-wavelength dispersive waves in the normal-GVD regime. The soliton number is a function of the characteristic dispersive and nonlinear length scales, given by $N = \sqrt{L_D/L_{NL}} = 10$. This corresponds to a soliton

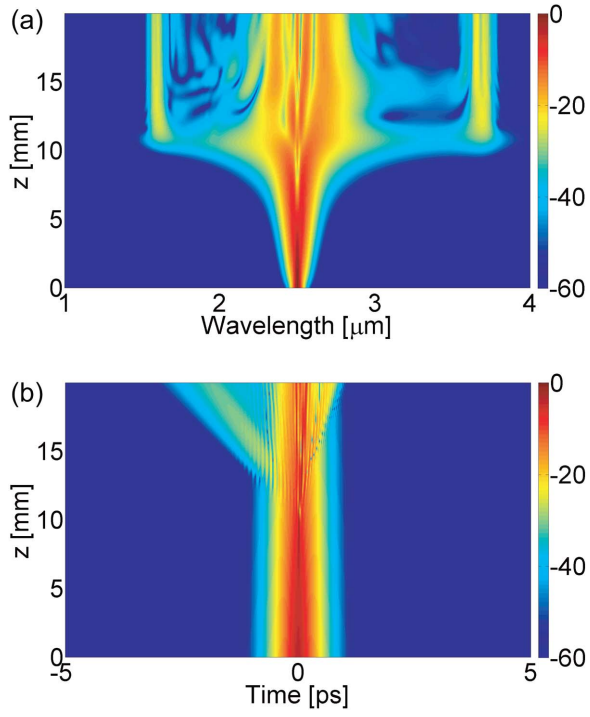

Fig. 3. Simulated (a) spectral and (b) temporal evolution versus propagation distance along the nanowaveguide for 2.5 μm pump and a coupled peak power of 15 W.

fission length of $L_{\text{fiss}} \approx L_D/N = 1$ cm, consistent with simulation results.

We numerically investigate the impact of 3PA, FCA, and FCD on SCG in the MIR region beyond 2.2 μm. Figure 4(a) shows a comparison of the various effects on the SCG output spectra from a 300 fs pulse with a peak power of $P_0 = 15$ W using parameters as given above. The dashed black line shows the output spectrum without 3PA ($\gamma_{3\text{PA}} = 0$). The dotted blue line corresponds to the case that includes 3PA but not free-carrier effects ($\gamma_{3\text{PA}} \neq 0$, σ, and $\mu = 0$), while the solid red line corresponds to the case that includes all nonlinear loss effects ($\gamma_{3\text{PA}}$, σ, $\mu \neq 0$). We note that the experimental results show that the telecom dispersive wave is much weaker than the corresponding MIR dispersive wave, whereas simulations predict both waves have comparable power levels. We attribute the relatively weak telecom dispersive wave to two effects. The first is the chromatic aberration of the collection optics and waveguide tapers, which are optimized for MIR wavelengths and thus reduce the power at telecom wavelengths received by the detector in the experiment. The second is the presence of TPA at telecom wavelengths, which is not included in simulations. We also note that the dynamic range of the FTIR is limited to 25 dB, so the weaker spectral features predicted by simulations are below the noise floor and not experimentally observable here.

For the power levels used in the experiment, the impact of 3PA, FCA, and FCD is not significant, as the overall spectral shape remains unchanged for the three plots shown in Fig. 4(a). To understand the impact of the various effects, we increase the pump power to $P_0 = 60$ W and show the simulated SCG results in Figs. 4(b)–4(d).

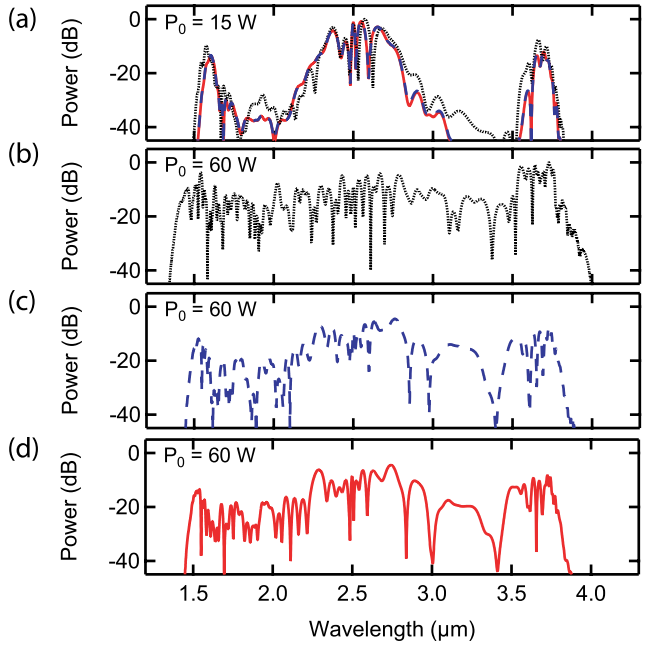

Fig. 4. (a) Simulated SCG output spectra from 2.5 μm pump with peak input power $P_0 = 15$ W. SCG output spectra with $P_0 = 60$ W for (b) no nonlinear loss mechanisms included (black dotted line), (c) only 3PA included (blue dashed line), and (d) full simulation with 3PA, FCA, and FCD included (red solid line). All plots have been normalized to the case with no nonlinear loss mechanisms (black dotted line).

Comparing Figs. 4(b) and 4(c), we find that 3PA is primarily responsible for a reduction in the total optical power, resulting in SCG with a lower peak power and narrower spectral bandwidth. We conclude that the generated free carriers do not significantly affect the SCG process, since they trail behind the pulse as it propagates along the waveguide.

The preceding analysis is valid for a pulsed source with a relatively low repetition rate such that the free carriers generated from a given pulse recombine before they can interact with subsequent pulses ($R_p \tau_{\text{eff}} < 1$). We now consider the case in which the repetition rate is on a time scale comparable to the free-carrier lifetime. We propagate a train of 50 pulses through the 2 cm waveguide and allow the generated carriers to accumulate between pulses until a steady state is reached. Figure 5(a) shows the resulting SCG spectrum for $P_0 = 15$ W and $R_p = 1$ GHz ($R_p \tau_{\text{eff}} = 10$), and Fig. 5(c) shows the carrier density along the length of the waveguide. Experimentally, the spectral gaps in our SCG spectrum are a result of the limited output power of our OPO; theoretically, an increase in pump power should result in broadband SCG. We simulate a pulse train of higher power ($P_0 = 60$ W, $R_p = 80$ MHz) including all nonlinear loss effects and plot the spectrum and carrier density in Figs. 5(b) and 5(d), respectively. In Fig. 5(b), the majority of carriers are generated halfway along the waveguide, corresponding to the onset of soliton fission and maximum pulse intensity. In Fig. 5(d), the majority of carriers are generated at the input of the waveguide, as the initial intensity of the pump pulse is higher.

In conclusion, we demonstrate SCG spectra spanning 1.3 octaves in a silicon nanowaveguide. By operating with the soliton fission length less than the length of the waveguide and with both ZGVD wavelengths near the pump, we achieve soliton fission and dispersive wave generation in both normal-GVD regimes. From our comprehensive analysis of multiphoton and free-carrier loss mechanisms, we conclude that they are not detrimental to SCG in the regime presented here. These results represent the first octave-spanning MIR SCG in silicon

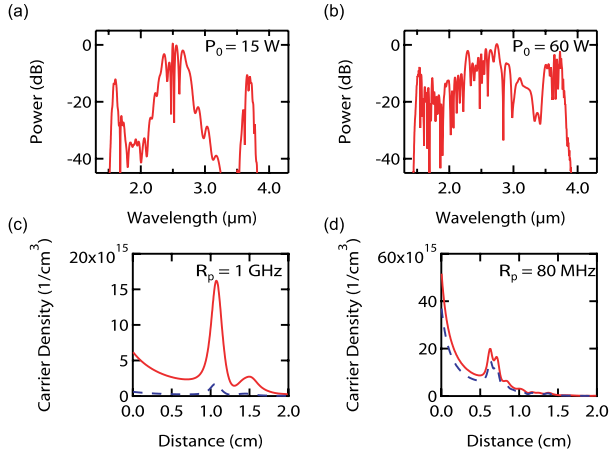

Fig. 5. Simulated SCG output spectra and carrier density along the length of the waveguide after 50 consecutive pulses using 2.5 μm pump with (a), (c) $R_p = 1$ GHz and $P_0 = 15$ W, and (b), (d) $R_p = 80$ MHz and $P_0 = 60$ W. Dashed blue lines show resulting carrier density for a single pulse.

as well as the longest wavelength generated via SCG within a silicon waveguide.

We acknowledge support from AFOSR under grant FA9550-12-1-0377 and the Defense Advanced Research Projects Agency via the PULSE program. This work was performed in part at the Cornell NanoScale Facility, a member of the National Nanotechnology Infrastructure Network, which is supported by the National Science Foundation (grant ECS-0335765).

References

1. A. V. Husakou and J. Herrmann, Phys. Rev. Lett. **87**, 4 (2001).
2. W. J. Wadsworth, A. Ortigosa-Blanch, J. C. Knight, T. A. Birks, T. P. M. Man, and P. S. Russell, J. Opt. Soc. Am. B **19**, 2148 (2002).
3. A. L. Gaeta, Opt. Lett. **27**, 924 (2002).
4. G. Genty, M. Lehtonen, H. Ludvigsen, and M. Kaivola, Opt. Express **12**, 3471 (2004).
5. J. M. Dudley, G. Genty, and S. Coen, Rev. Mod. Phys. **78**, 1135 (2006).
6. M. R. E. Lamont, B. Luther-Davies, D. Y. Choi, S. Madden, and B. J. Eggleton, Opt. Express **16**, 14938 (2008).
7. N. Granzow, S. P. Stark, M. A. Schmidt, A. S. Tverjanovich, L. Wondraczek, and P. S. J. Russell, Opt. Express **19**, 21003 (2011).
8. D. Duchesne, M. Peccianti, M. R. E. Lamont, M. Ferrera, L. Razzari, F. Legare, R. Morandotti, S. Chu, B. E. Little, and D. J. Moss, Opt. Express **18**, 923 (2010).
9. R. Halir, Y. Okawachi, J. S. Levy, M. A. Foster, M. Lipson, and A. L. Gaeta, Opt. Lett. **37**, 1685 (2012).
10. I. W. Hsieh, X. G. Chen, X. P. Liu, J. I. Dadap, N. C. Panoiu, C. Y. Chou, F. N. Xia, W. M. Green, Y. A. Vlasov, and R. M. Osgood, Opt. Express **15**, 15242 (2007).
11. B. Kuyken, X. P. Liu, R. M. Osgood, R. Baets, G. Roelkens, and W. M. J. Green, Opt. Express **19**, 20172 (2011).
12. U. D. Dave, S. Uvin, B. Kuyken, S. Selvaraja, F. Leo, and G. Roelkens, Opt. Express **21**, 32032 (2013).
13. A. D. Bristow, N. Rotenberg, and H. M. van Driel, Appl. Phys. Lett. **90**, 191104 (2007).
14. R. Claps, D. Dimitropoulos, V. Raghunathan, Y. Han, and B. Jalali, Opt. Express **11**, 1731 (2003).
15. S. Zlatanovic, J. S. Park, S. Moro, J. M. C. Boggio, I. B. Divliansky, N. Alic, S. Mookherjea, and S. Radic, Nat. Photonics **4**, 561 (2010).
16. R. K. W. Lau, M. Menard, Y. Okawachi, M. A. Foster, A. C. Turner-Foster, R. Salem, M. Lipson, and A. L. Gaeta, Opt. Lett. **36**, 1263 (2011).
17. X. P. Liu, R. M. Osgood, Y. A. Vlasov, and W. M. J. Green, Nat. Photonics **4**, 557 (2010).
18. B. Kuyken, X. P. Liu, G. Roelkens, R. Baets, R. M. Osgood, and W. M. J. Green, Opt. Lett. **36**, 4401 (2011).
19. G. P. Agrawal, *Nonlinear Fiber Optics* (Academic, 2006).
20. L. H. Yin, Q. Lin, and G. P. Agrawal, Opt. Lett. **32**, 391 (2007).
21. L. H. Yin and G. P. Agrawal, Opt. Lett. **32**, 2031 (2007).
22. F. Gholami, S. Zlatanovic, A. Simic, L. Liu, D. Borlaug, N. Alic, M. P. Nezhad, Y. Fainman, and S. Radic, Appl. Phys. Lett. **99**, 081102 (2011).
23. S. Pearl, N. Rotenberg, and H. M. van Driel, Appl. Phys. Lett. **93**, 131102 (2008).
24. R. A. Soref and B. R. Bennett, IEEE J. Quantum Electron. **23**, 123 (1987).
25. A. C. Turner-Foster, M. A. Foster, J. S. Levy, C. B. Poitras, R. Salem, A. L. Gaeta, and M. Lipson, Opt. Express **18**, 3582 (2010).